HDAC-6 inhibition ameliorates the early neuropathology in a mouse model of Krabbe disease

Sandra O. Braz[1†], Marlene M. Morgado[1†], Marta I. Pereira[1], Ana C. Monteiro[1], Olga Golonzhka[2], Matthew Jarpe[2], Pedro Brites[3], Monica M. Sousa[1*] and Joana Nogueira-Rodrigues[1*]

[1]Nerve Regeneration Group, Instituto de Biologia Molecular e Celular (IBMC), Instituto de Investigação e Inovação em Saúde (i3S), University of Porto, Porto, Portugal.

[2] Acetylon Pharmaceuticals Inc., Boston, MA 02118, United States.

[3]NeuroLipid Biology Group, Instituto de Biologia Molecular e Celular (IBMC), Instituto de Investigação e Inovação em Saúde (i3S), University of Porto, Porto, Portugal.

*** Correspondence:**
Joana Nogueira-Rodrigues
joana.rodrigues@ibmc.up.pt
Monica M Sousa
msousa@ibmc.up.pt

† These authors contributed equally to this work and share first authorship

Number of words: 3681

Number of figures: 5

Abstract

In Krabbe disease (KD), mutations in β-galactosylceramidase (GALC), a lysosomal enzyme responsible for the catabolism of galactolipids, lead to the accumulation of its substrates galactocerebroside and psychosine. This neurologic condition is characterized by a severe and progressive demyelination together with neuron-autonomous defects and degeneration. Twitcher mice mimic the infantile form of KD, which is the most common form of the human disease. The Twitcher CNS and PNS present demyelination, axonal loss and neuronal defects including decreased levels of acetylated tubulin, decreased microtubule stability and impaired axonal transport. Here, we tested whether inhibiting the α-tubulin deacetylase HDAC6 with a specific inhibitor, ACY-738, was able to counteract the early neuropathology and neuronal defects of Twitcher mice. Our data show that delivery of ACY-738 corrects the low levels of acetylated tubulin in the Twitcher nervous system. Furthermore, it reverts the loss myelinated axons in the sciatic nerve and in the optic nerve when administered from birth to postnatal day 9, suggesting that the drug holds neuroprotective properties. The extended delivery of ACY-738 to Twitcher mice delayed axonal degeneration in the CNS and ameliorated the general presentation of the disease. ACY-738 was effective in rescuing neuronal defects of Twitcher neurons, stabilizing microtubule dynamics and increasing the axonal transport of mitochondria. Overall, our results support that ACY-738 has a neuroprotective effect in KD and should be considered as an add-on therapy combined with strategies targeting metabolic correction.

Keywords: axonal transport, HDAC6, Krabbe disease, leukodystrophy, microtubule stability, tubulin acetylation, Twitcher mice.

This is a provisional file, not the final typeset article

1 INTRODUCTION

Krabbe disease (KD), or globoid cell leukodystrophy, is a lysosomal storage disorder caused by mutations in the *galc* gene that result in impaired activity of the lysosomal hydrolase galactosylceramidase (GALC). As a consequence of GALC deficiency, the metabolism of several galactosphingolipids is impaired and GALC substrates - galactosylceramide and galactosylsphingosine (also known as psychosine), accumulate (Wenger et al., 1997). Whereas galactocerebroside builds up inside macrophages and microglia giving rise to globoid cells, psychosine is highly toxic to myelin-forming cells (oligodendrocytes in the central nervous system - CNS - and Schwann cells in the peripheral nervous system - PNS). Psychosine disrupts the architecture and composition of lipid rafts (White et al., 2009) and leads to the activation of apoptosis pathways that result in progressive demyelination (Zaka and Wenger, 2004, Miyatake and Suzuki, 1972, Krabbe, 1916, Igisu and Suzuki, 1984). Consequently, KD patients present severe irritability, limb stiffness, motor function impairment, mental development arrest, epileptic seizures, hypertonicity and dystonia (Krabbe, 1916, Bradbury et al., 2021). Among the KD onsets based on the age of presentation of symptoms, the infantile onset is the most prevalent and severe subtype, as patients usually do not survive past 2 years of age (Hagberg et al., 1969, Bradbury et al., 2021). The Twitcher mouse, a naturally occurring mutant with a premature stop codon in the *galc* gene that results in lack of functional GALC (Suzuki and Suzuki, 1995), mimics the infantile form of KD (Lee et al., 2006). Similarly to human patients, Twitcher mice present demyelination both in the CNS and PNS that can be clearly detected at post-natal day 15 (P15) (Tanaka et al., 1988).

Hematopoietic stem cell transplantation (HSCT) emerged as one of the most valuable treatments for KD, delaying disease progression and extending life time of KD patients if transplantation is performed before the onset of symptoms (Escolar et al., 2005, Kreher et al., 2022). Further than being a possible source of GALC, HSCT may produce a neuroprotective effect by reducing neuroinflammation (Qin et al., 2012). In spite of co-morbidities, HSCT slows down disease progression and improves pathology in the CNS, while a less significant effect is observed in the PNS, possibly given the limited cross-correction of Schwann cells (Wright et al., 2017, Kofler et al., 2022). Due to the advances on the clinical use of engineered AAV capsids capable of penetrating the blood brain barrier, two AAV-based clinical trials for KD (NCT04693598 and NCT04771416) are currently underway (Heller et al., 2023). While NCT04771416 is assessing the efficacy of *Galc* delivery into the cisterna magna using a modified AAV9 vector, NCT04693598 is testing the combined effect of HSCT and *Galc* i.v. delivery using AAVrh10. In fact, it is likely that future therapeutic approaches for KD will rely on combinatorial strategies aimed at providing the missing enzyme and simultaneously counteract neuroinflammation and promote neuroprotection.

In respect to neuroprotection, it is important to note that in addition to demyelination, neuronal-autonomous defects are also central players in KD progression (Kreher et al., 2022, Brites and Sousa, 2022). In fact, a myelin-independent axonopathy contributes to the severe neuropathology in Twitcher mice (Castelvetri et al., 2011, Smith et al., 2011, Teixeira et al., 2014, Kreher et al., 2022), correlating with reports of loss of unmyelinated axons in human KD nerves (Sourander and Olsson, 1968). Our group has shown that before the onset of demyelination, Twitcher mice already exhibit a decreased number of axons in the CNS and PNS, and of sensory neurons in dorsal root ganglia (Teixeira et al., 2014). In fact, Twitcher neurons have a generalized impairment in axonal transport including mitochondria (Cantuti Castelvetri et al., 2013), lysosomes (Teixeira et al., 2014) and synaptic vesicles (Teixeira et al., 2014), possibly associated with abnormal levels of post-translational modifications of tubulin and with a decreased microtubule stability (Teixeira et al., 2014). Of note, in Twitcher mice, microtubules have decreased levels of polyglutamylated and acetylated tubulin (Teixeira et al., 2014), which may be directly linked with the defective axonal transport.

α-tubulin acetylation is tightly regulated by α-tubulin-acetyltransferases (αTATs) and a specific histone deacetylase, HDAC6, that has a cytoplasmic location and thereby does not interfere with histone acetylation (Hubbert et al., 2002). Studies using HDAC6 inhibitors highlighted their neuroprotective role as they facilitate axonal transport by promoting microtubule acetylation (Zilberman et al., 2009, Chen et al., 2010, Dompierre et al., 2007, Rivieccio et al., 2009). This is especially relevant in KD, as Twitcher mice have impaired axonal transport and diminished levels of acetylated tubulin (Teixeira et al., 2014). Several HDAC6 inhibitors have been used in various models of neurodegeneration such as tubastatin A (Jian et al., 2017), trichostatin A (Su et al., 2021), ACY-775 (Benoy et al., 2017) and ACY-738 (Rossaert et al., 2019). ACY-738 (N-hydroxy-2-(1-phenylcycloproylamino)pyrimidine-5-carboxamide) inhibits the C- terminal catalytic domain of HDAC6, increasing α-tubulin acetylation without altering histone acetylation (Jochems et al., 2014). Although this compound has a rapid elimination from plasma, upon systemic administration, it leads to sufficient brain exposure, crossing the BBB (Jochems et al., 2014, Majid et al., 2015). Thus, ACY-738 targets HDAC6 function in the CNS. Indeed, ACY-738 treatment of a mouse model of multiple sclerosis increases short-term memory and decelerates disease progression (LoPresti, 2019). Current data indicates that ACY-738 promotes axon growth *in vitro* in inhibitory conditions (Rivieccio et al., 2009), and *in vivo* improves the outcome of animal models of several neurodegenerative conditions (Majid et al., 2015, LoPresti, 2019, Benoy et al., 2017, Rossaert et al., 2019, Burg et al., 2021). As stable microtubules are the railroads for axonal cargos, ACY-738 is also associated with increased efficiency of axonal transport (Majid et al., 2015, Guo et al., 2017).

Given the impairment the defect in tubulin acetylation in Twitcher nerves, we tested whether ACY-738 delivery could counteract the early neuropathology of this KD model. Here, we show that the early systemic delivery of ACY-738 robustly increases tubulin acetylation, stabilizes microtubule dynamics, increases axonal transport, and rescues the early loss of myelinated axons in the optic and sciatic nerves of Twitcher mice. Our results thus support that ACY-738 has neuroprotective effect in KD and should be considered as an add-on therapy in KD.

MATERIALS AND METHODS

Animals

Twitcher (twi) mice and wild-type (WT) littermates were obtained from heterozygous breeding pairs (Jackson Laboratory). Genotyping of Twitcher mice was based on the use of a PCR mismatched primer that creates a restriction site for EcoRV if the *Galc* allele possesses the mutation, as described (Sakai et al., 1996). Mice were bred at the i3S animal facility with *ad libitum* access to water and rodent food, and were kept on a 12 hour light and dark cycle. All mice were handled and euthanized according to the i3S humane endpoints standard operation procedure established according to FELASA's recommendations (www.felasa.eu) when any of the following features was observed: persistent lethargy and paralysis, severely impaired mobility, prolonged dehydration (for more than 72 hours) or severe weight loss (more than 20%) arising from inability of drinking or eating. After weaning, Twitcher mice were fed with accessible wet rodent's chow and supplemented with Anima-Strath.

Functional evaluation

Animals were monitored twice per week until P25 and then daily until humane endpoints were reached. Parameters including weight loss, natural/provoked behavior, and activity level were scored. Natural behavior was assessed by observation of the animal in its home cage; animals with normal mobility

This is a provisional file, not the final typeset article

138 and alert received the highest score (3) whereas less motile and not alert animals did not score (0). The
139 animals were then touched to provoke a response, which was scored with 3 if the animal reacted
140 normally or less if the response was weaker or absent (0).

141

142 **Subcutaneous delivery of ACY-738**

143 ACY-738 (Acetylon Pharmaceuticals) was prepared in 0.5% hydroxypropyl methylcellulose (HPMC)
144 diluted in PBS at a final concentration of 0.5 mg/ml. Starting at P0, Twitcher mice were injected
145 subcutaneously every day (3mg/kg) with either ACY-738 (in 0.5% HPMC) or vehicle (0.5% HPMC)
146 and euthanized at P9 (n=10 for each condition) or maintained until humane endpoints were reached
147 (n=10-14 animals for each condition). WT mice were also injected subcutaneously daily with ACY-
148 738 (n=8-10) or vehicle (n=8-10) to serve as controls. Either at P9 or when animals reached humane
149 endpoints, brains, sciatic nerves, optic nerves and dorsal root ganglia (DRG) were collected and
150 processed for morphometric analysis, western blot analysis or primary neuron cultures, as described
151 below. During the delivery period, no signs of toxicity of the drug were detected.

152

153 **Western blot analysis**

154 Sciatic nerves, optic nerves and brains from ACY-738-treated Twitcher mice (n=10) or control
155 Twitcher mice (n=8-9) were homogenized in lysis buffer (PBS containing 0.3% Triton X-100, 1 mM
156 sodium orthovanadate and protease inhibitors (Roche, 4693132001). Total protein of each sample was
157 determined using the Bio-Rad DC kit (Bio-Rad, 5000116) and protein lysates were run on 10% SDS-
158 PAGE (5µg/lane) and transferred to supported nitrocellulose membranes (Amersham, 10600013).
159 Membranes were incubated overnight at 4°C with mouse anti-acetylated tubulin (1:20,000; Sigma,
160 T7451) and mouse anti-α-tubulin (1:10,000; Sigma, T6199). Secondary antibody were HRP-
161 conjugated anti-mouse IgG (1:5,000; Jackson ImmunoResearch, 115-035-003) or the IRDye® 800CW
162 Goat anti-Mouse IgG (1:5000; LI-COR, 926-32210). Proteins were detected using Luminata Forte
163 (Millipore, WBLUR0500) and quantification was performed by densitometry using QuantityOne
164 software (Bio-Rad). Alternatively, the Odyssey CLx (LI-COR) imaging system was used for detection
165 of membrane total protein (926-11010) and dye-conjugated labelled secondary antibodies (926-32212
166 and 926-68073).

167

168 **Neuropathological analysis**

169 For each animal (both in the case of ACY-738 delivery from P0 to P9 and from P0 until humane
170 endpoints (n=8 ACY-738-treated and n=8 control Twitcher mice), the right sciatic and optic nerves
171 were used for neuropathological analyses. All tissues were isolated and fixed by immersion in 4%
172 glutaraldehyde in 0.1M sodium cacodylate buffer (pH 7.4) for 5 days and processed as previously
173 described (da Silva et al., 2014). To determine the number of myelinated axons, 1µm-thick transverse
174 sections covering the complete cross-sectional area of the sciatic nerve were stained with p-phenylene-
175 diamine (PPD) and the total number of myelinated axons was counted. For g-ratio analysis, the axonal
176 diameter and the myelin sheath thickness were measured by dividing the diameter of each axon by its
177 myelin-including diameter (80-150 fibers per animal). To determine the density of unmyelinated
178 axons, ultrathin transverse sciatic nerve sections (50 nm) were cut, stained with uranyl acetate and lead
179 citrate and 10 non-overlapping photomicrographs (5,000x magnification) were taken in a transmission
180 electron microscope (JEOL 100CX II). The optic nerve was treated similarly and myelinated and
181 unmyelinated axons were counted from ultrathin transverse nerve sections. In all measurements, the
182 observer was blinded to the experimental condition.

183

184 **Primary culture of dorsal root ganglia (DRG) neurons**

185 DRG were isolated from WT and Twitcher mice at P9 or when human endpoints were reached. Ganglia
186 were collected to DMEM:F12 (Sigma-Aldrich, D8437) supplemented with 10% fetal bovine serum
187 (FBS; Sigma-Aldrich, F9665) and 1% penicillin/streptomycin (P/S; Invitrogen, 15140-122). DRG
188 were digested with collagenase IV-S (Sigma-Aldrich, C1889) for 1 hour and 30 minutes. Neurons were
189 isolated centrifuging the cell suspension into a 15% bovine serum albumin (BSA; Sigma-Aldrich,
190 A3294) cushion, for 10 minutes at 1000 rpm. Cells were resuspended on DMEM:F12 supplemented
191 with 1% P/S, 2× B27 (Invitrogen, 0080085SA), 2 mM L-glutamine (L-Glu; Invitrogen, 25030024) and
192 50 ng/mL nerve growth factor (NGF; Merck Millipore, 01-125).

193

194 **Assessment of microtubule dynamics**

195 For the analysis of microtubule dynamics in the growth cone, adult DRG neurons from Twitcher and
196 WT mice were isolated as described above and nucleofected with a plasmid encoding pEGFP-eEB3
197 (Addgene #190164). After transfection, cells were left in suspension for 24h. At DIV1, cells were
198 plated at a density of 10,000 cells/well in glass-bottom 8-well μ-dishes. At DIV5, two hours before
199 imaging, half of the medium was replaced with complete media without phenol red and supplemented
200 with 100 nM ACY-738 in 0.1% DMSO or 0.1% DMSO alone. Transfected cells were visualized using
201 the 100x objective of a spinning disk confocal system Andor Revolution XD with an iXonEM+ DU-
202 897 camera and IQ 1.10.1 software (ANDOR Technology). Time-lapse recordings (a total of 60
203 frames, every 2 seconds) were acquired in three planes separated by 0.2 μm each at 37°C and 5% CO2.
204 For the quantification of EB3 comet growth speed, kymographs were performed using the Fiji
205 KymoResliceWide plugin (distance, x axis; time, y axis). Starting and end positions of the traces were
206 defined using the Fiji Cell Counter plugin.

207

208 **Analysis of axonal transport**

209 For live imaging of axonal transport, DRG neurons from ACY-738-treated and control mice were
210 isolated as previously described. Dissociated DRG neurons (4,000 cells/well) were cultured in
211 DMEM:F12 supplemented with NGF, Pen/Strep, B27 and L-glutamine for 16 hours in 8-well μ-slides
212 ibiTreat (Ibidi) coated with PLL and laminin. DRG neurons isolated from ACY-738-treated WT and
213 Twitcher mice were maintained in culture in the presence of 100 nM ACY-738 in 0.1% DMSO. Control
214 WT and Twitcher DRG neurons were maintained in 0.1% DMSO. For the analysis of axonal transport
215 of mitochondria, DRG neurons were incubated with Mitotracker (Invitrogen, M7510) in DMEM:F12
216 for 45 min at 37°C. Axonal transport was visualized in a confocal SP5II Leica microscope.
217 Photomicrographs were taken for 2 min with 1 sec frame intervals with 5 Z-stacks per frame. For each
218 condition, the movement of at least 50 organelles was tracked. Analysis of axonal transport (velocity
219 and flux) was done using the Fiji software.

220

221 **Quantification and statistical analysis**

222 Data is shown as mean and standard error of the mean (SEM). The statistical analysis for all
223 experiments was performed with GraphPad Prism 6. Unless elsewhere stated, the following statistical
224 tests were used as indicated in figure legends: two-tailed unpaired t-test, one-way or two-way ANOVA
225 followed by Tukey's multiple comparison test. Sample sizes are indicated in figure legends and
226 significance was defined as p value*<0.05, p**<0.01, p***<0.001, p****<0.0001, ns: not significant.

This is a provisional file, not the final typeset article

227

228

229 ## 2 RESULTS

230 **ACY-738 subcutaneous delivery increases tubulin acetylation in the nervous tissue of Twitcher**
231 **mice**

232 To test the possible neuroprotective effect of ACY-738 in KD, the drug was delivered subcutaneously
233 daily to Twitcher mice. Since Twitcher mice present axonal loss that can be detected readily at P9,
234 prior to the onset of demyelination (Teixeira et al., 2014), we explored the potential beneficial effects
235 of ACY-738 delivery from P0 to P9 (Figure 1A). We analyzed the levels of tubulin acetylation in
236 brains, optic and sciatic nerves from P9 ACY-738-treated Twitcher mice. As expected from the
237 capacity of ACY-738 to penetrate the nervous system (Jochems et al., 2014), all tissues had increased
238 levels of acetylated tubulin in ACY-738-treated Twitcher mice (9-, 2- and 4-fold, respectively) (Figures
239 1B-D). In all the above tissues, no differences were seen in the levels of other tubulin modifications
240 including tyrosinated and de-tyrosinated tubulin resulting from ACY-738 treatment (data not shown).
241 We then extended our analysis of ACY-738 effect on Twitcher mice treated until humane endpoints
242 were reached (Figure 1E). At this timepoint, untreated Twitcher mice had decreased levels of acetylated
243 tubulin in the brain (Figure 1F) and optic nerve (Figure 1G). In the sciatic nerve, in support of our
244 previous observations at P9 (Teixeira et al., 2014), at humane endpoints a tendency for decreased
245 tubulin acetylation in Twitcher mice persisted (Figure 1H). ACY-738 treatment resulted in increased
246 tubulin acetylation in all the examined tissues of Twitcher mice (Figures 1F-G). Collectively our data
247 show that Twitcher mice have decreased acetylated tubulin levels throughout the nervous system that
248 can be reverted by ACY-738 systemic delivery.

249

250 **ACY-738 stabilizes microtubule dynamics and increases the axonal transport of mitochondria in**
251 **Twitcher DRG neurons**

252 Twitcher neurons exhibit decreased acetylated tubulin levels, decreased microtubule cytoskeleton
253 stability (Teixeira et al., 2014), and impaired axonal transport (Cantuti Castelvetri et al., 2013). Since
254 microtubule stability is required for efficient axonal transport (Kapitein and Hoogenraad, 2015), drugs
255 that target microtubule acetylation may be useful candidates to improve the neuropathological
256 presentation of KD. As such, we explored whether ACY-738 was able to stabilize the microtubule
257 cytoskeleton and increase the axonal transport of Twitcher DRG neurons. We started by analyzing
258 microtubule dynamics of Twitcher DRG neurons in the presence of ACY-738. Both in the growth cone
259 and in the axon shaft, ACY-738 decreased microtubule growth speed of treated Twitcher DRG neurons
260 (Figure 2A), while in treated WT this effect was restricted to the axon shaft, supporting the powerful
261 role of ACY-738 in stabilizing the microtubule cytoskeleton. As previously reported (Teixeira et al.,
262 2014), Twitcher neurons exhibited a higher microtubule growth speed comparing with WT neurons,
263 which was rescued by the treatment with ACY-738 (Figure 2A). Of note, no differences were observed
264 in EB3 comet density (data not shown).

265 As axonal transport efficiency is highly influenced by microtubule organization and dynamics
266 (Kapitein and Hoogenraad, 2015), we hypothesized that the disruption of axonal transport observed in
267 Twitcher mice might be recovered by ACY-738 treatment. In DRG from animals treated until humane
268 endpoints, in agreement with previous reports (Cantuti Castelvetri et al., 2013, Teixeira et al., 2014),
269 Twitcher DRG neurons exhibited a decreased mitochondia velocity both in the anterograde and
270 retrograde direction that was reverted by ACY-738 treatment to the WT levels (Figure 2B). ACY-

271 738-treatment did not interfere with the axonal transport of mitochondria in WT animals (Figure 2B).
272 Overall, our data show that ACY-738 is a valuable cytoskeleton-targeting drug to correct defects in
273 microtubule cytoskeleton dynamics and rescue the impaired mitochondrial axonal transport of
274 Twitcher DRG neurons.

275

276 **Twitcher mice treated with ACY-738 have improved functional performance**

277 Twitcher mice develop tremors at around 18-20 days of age and muscle weakness and weight loss at
278 P20-25 and usually reach the humane endpoints established in our facility (and recommended by
279 FELASA) at 30-35 days of age. To determine the possible effect of ACY-738 treatment in disease
280 progression, animals were monitored daily for their functional performance. ACY-738-treatment
281 resulted in a substantial improvement of natural (Figure 3A) and provoked behavior (Figure 3B) and
282 in increased activity levels (Figure 3C). Despite the general improvement in function, mobility and
283 activity induced by ACY-738 treatment, on its own the drug did not result in an overall increased
284 average lifespan (average of 32 days for untreated and treated Twitcher mice).

285

286 **ACY-738 delivery rescues the early loss of myelinated axons in the Twitcher CNS and PNS**

287 Given the functional improvement of Twitcher mice treated with ACY-738, we further investigated its
288 potential to correct the early neuropathology of this model. In the optic nerve, as previously reported
289 (Teixeira et al., 2014), P9 Twitcher mice exhibited a decreased density of myelinated fibers when
290 compared with WT nerves (Figure 4A-B). Notably, ACY-738 treatment increased the density of
291 myelinated axons of Twitcher mice partially rescuing the defect of Twitcher optic nerves (Figure 4B).
292 Moreover, the decreased myelin thickness in Twitcher mice was rescued by ACY-738 treatment, as
293 determined by g-ratio analysis (Figure 4C). In the case of unmyelinated axons, their increased density
294 in the optic nerve of Twitcher mice was unchanged by ACY-738 treatment (Figure 4D).

295 Similar to the optic nerve, P9 Twitcher sciatic nerves displayed a reduced density of both
296 myelinated and unmyelinated axons in comparison with WT sciatic nerves (Figure 4E-G), as
297 previously described by our group (Teixeira et al., 2014). ACY-738 treatment normalized the density
298 of myelinated axons of Twitcher sciatic nerves, as following treatment values were similar to those of
299 WT sciatic nerves (Figure 4F). However, unlike the optic nerve, in the case of the sciatic nerve, ACY-
300 738 treatment did not rescue the decreased myelin thickness (data not shown). Similar to the optic
301 nerve, ACY-738 did not rescue the defect of unmyelinated axons in Twitcher sciatic nerves (Figure
302 4G). In summary, our data shows that ACY-738 treatment rescues specifically the early loss of
303 myelinated axons in Twitcher mice, both in the CNS (optic nerve) and PNS (sciatic nerve).

304

305 **Extended delivery of ACY-738 reverts the optic nerve neuropathology of Twitcher mice**

306 The results obtained from the subcutaneous delivery of ACY-738 from P0-P9 warranted the analysis
307 of treated Twitcher mice for extended time periods, i.e. until humane endpoints were reached. Detailed
308 analysis of control and ACY-738-treated Twitcher mice showed that the number of small caliber
309 myelinated axons was increased by ACY-738 treatment (Figure 5A). Specifically, ACY-738 treatment
310 resulted in a partial rescue of the density of myelinated axons in the optic nerve to the levels of those
311 observed in WT animals (Figure 5A-B). Myelin thickness in Twitcher optic nerves was decreased in
312 comparison with WT, a defect that was attenuated upon ACY-738 delivery (Figure 5C). Interestingly,
313 with longer delivery times, ACY-738 was able to revert the high density of unmyelinated axons of
314 Twitcher mice, to that observed in WT optic nerves (Figure 5D). In Twitcher sciatic nerves, despite
315 the benefits at early time points post-delivery, the density of both myelinated (Figure 5E-F) and

This is a provisional file, not the final typeset article

316 unmyelinated axons (Figure 5G) was unchanged by ACY-738 treatment. Together our data shows that
317 the delivery of ACY-738 to Twitcher mice up to human endpoints is capable of reverting the
318 neuropathology in the optic nerve whereas the sciatic nerve correction is not achieved.

319

320

321 **3 DISCUSSION**

322 KD is a severe neurological condition for which therapeutic options are still limited and mainly focused
323 on managing symptomatology. The current standard therapy – HSCT – that provides for GALC cross-
324 correction and reduction of neuroinflammation, has inherent co-morbidities and an efficacy that is
325 mostly restricted to asymptomatic KD children (Escolar et al., 2005). Even in successful cases, years
326 after HSCT some patients develop severe peripheral neuropathy (Wright et al., 2017, Siddiqi et al.,
327 2006). Given the ability of specific AAV serotypes to cross the blood-brain barrier (Chan et al., 2017),
328 these are becoming the option of choice for gene delivery in monogenic disorders where the nervous
329 system is affected. However, in long-surviving AAV-treated Twitcher mice, multiple demyelinating
330 areas are still detected in the brain, suggesting a possible late onset reduction of AAV efficacy (Heller
331 et al., 2021). Recently, the combination of HSCT with AAV-mediated gene therapy proved to have
332 synergistic effects in animal models of KD (Rafi et al., 2015, Lin et al., 2007) and is currently under
333 evaluation in a clinical trial (NCT04693598). The current knowledge on KD strongly points towards
334 the possibility that long-term effective therapies targeting different aspects of the pathology and
335 different groups of patients, will most probably rely on combinatorial approaches.
336 Although KD shares many features with other leukodystrophies, myelin-independent neuronal
337 defects are also responsible for the severe neuropathology observed in Twitcher mice (Castelvetri et
338 al., 2011, Smith et al., 2011, Teixeira et al., 2014, Kreher et al., 2022). A considerable body of evidence
339 supports that defects in the neuronal cytoskeleton may be part of the initial steps of neurodegeneration
340 in KD (Nogueira-Rodrigues et al., 2016). The knowledge gained on the dysregulated molecular events
341 in KD neurons opens exciting new windows of action to counteract the associated neuropathology.
342 Given the reduced levels of acetylated tubulin in Twitcher nerves, we tested whether targeting the
343 microtubule acetylation enzyme HDAC6 through the delivery of a specific inhibitor, ACY-738, was
344 able to counteract the early axonal loss observed in this model. Considering its properties, ACY-738
345 is a strong therapeutic candidate for KD since it displays brain bioavailability upon systemic
346 administration, low nanomolar potency and high selectivity in comparison with other HDAC6
347 inhibitors (Jochems et al., 2014), with the potential of correcting the low levels of acetylated tubulin
348 present in Twitcher nerves. Of note, ACY-738 has been established as a neuroprotective molecule in
349 other neurodegenerative conditions, improving neuropathology and disease presentation in Charcot-
350 Marie Tooth disease and multiple sclerosis (Benoy et al., 2017, LoPresti, 2019). Here, we show that
351 the early systemic delivery of ACY-738 robustly increases tubulin acetylation in the nervous tissue of
352 Twitcher mice, promoting microtubule stability, increasing axonal transport, and improving functional
353 performance. From the neuropathological standpoint, ACY-738 delivery rescues the early loss of
354 myelinated axons in the optic and sciatic nerves of Twitcher mice. Additionally, induced and sustained
355 myelination will also contribute to maintain axon health and prevent neurodegeneration. In summary,
356 our results support that ACY-738 has a neuroprotective effect in KD and should be further tested as an
357 add-on therapy combined with strategies targeting metabolic correction.

358

359 **4 CONFLICT OF INTEREST**

The Nerve Regeneration group was supported by a Sponsored Research Agreement with Acetylon Pharmaceuticals Inc that provided ACY-738.

5 AUTHOR CONTRIBUTIONS

M.M.S and J.N-R. coordinated research. M.J., M.M.S and J.N-R. designed the study. S.O.B, P.B., M.J. M.M.S. and J. N-R analysed experiments. S.O.B., M.M.M., M.I.P, A.C.M and J.N.R. performed the experiments. S.O.B, M.M.S and J.N-R. wrote the manuscript.

6 FUNDING

Work was supported by a Sponsored Research Agreement with Acetylon Pharmaceuticals Inc.

7 ACKNOWLEDGMENTS

We thank the support of the i3S Scientific Platforms (Animal, Histology and Electron Microscopy, Advanced Light Microscopy and BioSciences Screening Facilities, part of the national infrastructure PPBI - Portuguese Platform of Bioimaging; PPBI-POCI-01-0145-FEDER-022122).

8 REFERENCES

BENOY, V., VANDEN BERGHE, P., JARPE, M., VAN DAMME, P., ROBBERECHT, W. & VAN DEN BOSCH, L. 2017. Development of Improved HDAC6 Inhibitors as Pharmacological Therapy for Axonal Charcot-Marie-Tooth Disease. *Neurotherapeutics,* 14**,** 417-428.

BRADBURY, A. M., BONGARZONE, E. R. & SANDS, M. S. 2021. Krabbe disease: New hope for an old disease. *Neurosci Lett,* 752**,** 135841.

BRITES, P. & SOUSA, M. M. 2022. Neurons contribute to pathology in a mouse model of Krabbe disease in a cell-autonomous manner. *PLoS Biol,* 20**,** e3001706.

BURG, T., ROSSAERT, E., MOISSE, M., VAN DAMME, P. & VAN DEN BOSCH, L. 2021. Histone Deacetylase Inhibition Regulates Lipid Homeostasis in a Mouse Model of Amyotrophic Lateral Sclerosis. *Int J Mol Sci,* 22.

CANTUTI CASTELVETRI, L., GIVOGRI, M. I., HEBERT, A., SMITH, B., SONG, Y., KAMINSKA, A., LOPEZ-ROSAS, A., MORFINI, G., PIGINO, G., SANDS, M., BRADY, S. T. & BONGARZONE, E. R. 2013. The sphingolipid psychosine inhibits fast axonal transport in Krabbe disease by activation of GSK3beta and deregulation of molecular motors. *J Neurosci,* 33**,** 10048-56.

CASTELVETRI, L. C., GIVOGRI, M. I., ZHU, H., SMITH, B., LOPEZ-ROSAS, A., QIU, X., VAN BREEMEN, R. & BONGARZONE, E. R. 2011. Axonopathy is a compounding factor in the pathogenesis of Krabbe disease. *Acta Neuropathol,* 122**,** 35-48.

CHAN, K. Y., JANG, M. J., YOO, B. B., GREENBAUM, A., RAVI, N., WU, W. L., SANCHEZ-GUARDADO, L., LOIS, C., MAZMANIAN, S. K., DEVERMAN, B. E. & GRADINARU, V. 2017. Engineered AAVs for efficient noninvasive gene delivery to the central and peripheral nervous systems. *Nat Neurosci,* 20**,** 1172-1179.

CHEN, S., OWENS, G. C., MAKARENKOVA, H. & EDELMAN, D. B. 2010. HDAC6 regulates mitochondrial transport in hippocampal neurons. *PLoS One,* 5**,** e10848.

DA SILVA, T. F., EIRA, J., LOPES, A. T., MALHEIRO, A. R., SOUSA, V., LUOMA, A., AVILA, R. L., WANDERS, R. J., JUST, W. W., KIRSCHNER, D. A., SOUSA, M. M. & BRITES, P. 2014. Peripheral nervous system plasmalogens regulate Schwann cell differentiation and myelination. *J Clin Invest,* 124**,** 2560-70.

DOMPIERRE, J. P., GODIN, J. D., CHARRIN, B. C., CORDELIERES, F. P., KING, S. J., HUMBERT, S. & SAUDOU, F. 2007. Histone deacetylase 6 inhibition compensates for the transport deficit in Huntington's disease by increasing tubulin acetylation. *J Neurosci,* 27**,** 3571-83.

This is a provisional file, not the final typeset article

402 ESCOLAR, M. L., POE, M. D., PROVENZALE, J. M., RICHARDS, K. C., ALLISON, J., WOOD, S., WENGER, D. A.,
403 PIETRYGA, D., WALL, D., CHAMPAGNE, M., MORSE, R., KRIVIT, W. & KURTZBERG, J. 2005.
404 Transplantation of umbilical-cord blood in babies with infantile Krabbe's disease. *N Engl J Med,* 352**,**
405 2069-81.
406 GUO, W., NAUJOCK, M., FUMAGALLI, L., VANDOORNE, T., BAATSEN, P., BOON, R., ORDOVAS, L., PATEL, A.,
407 WELTERS, M., VANWELDEN, T., GEENS, N., TRICOT, T., BENOY, V., STEYAERT, J., LEFEBVRE-OMAR, C.,
408 BOESMANS, W., JARPE, M., STERNECKERT, J., WEGNER, F., PETRI, S., BOHL, D., VANDEN BERGHE, P.,
409 ROBBERECHT, W., VAN DAMME, P., VERFAILLIE, C. & VAN DEN BOSCH, L. 2017. HDAC6 inhibition
410 reverses axonal transport defects in motor neurons derived from FUS-ALS patients. *Nat Commun,* 8**,**
411 861.
412 HAGBERG, B., KOLLBERG, H., SOURANDER, P. & AKESSON, H. O. 1969. Infantile globoid cell leucodystrophy
413 (Krabbe's disease). A clinical and genetic study of 32 Swedish cases 1953--1967. *Neuropadiatrie,* 1**,**
414 74-88.
415 HELLER, G., BRADBURY, A. M., SANDS, M. S. & BONGARZONE, E. R. 2023. Preclinical studies in Krabbe
416 disease: A model for the investigation of novel combination therapies for lysosomal storage diseases.
417 *Mol Ther,* 31**,** 7-23.
418 HELLER, G. J., MARSHALL, M. S., ISSA, Y., MARSHALL, J. N., NGUYEN, D., RUE, E., PATHMASIRI, K. C.,
419 DOMOWICZ, M. S., VAN BREEMEN, R. B., TAI, L. M., COLOGNA, S. M., CROCKER, S. J., GIVOGRI, M. I.,
420 SANDS, M. S. & BONGARZONE, E. R. 2021. Waning efficacy in a long-term AAV-mediated gene
421 therapy study in the murine model of Krabbe disease. *Mol Ther,* 29**,** 1883-1902.
422 HUBBERT, C., GUARDIOLA, A., SHAO, R., KAWAGUCHI, Y., ITO, A., NIXON, A., YOSHIDA, M., WANG, X. F. &
423 YAO, T. P. 2002. HDAC6 is a microtubule-associated deacetylase. *Nature,* 417**,** 455-8.
424 IGISU, H. & SUZUKI, K. 1984. Progressive accumulation of toxic metabolite in a genetic leukodystrophy.
425 *Science,* 224**,** 753-5.
426 JIAN, W., WEI, X., CHEN, L., WANG, Z., SUN, Y., ZHU, S., LOU, H., YAN, S., LI, X., ZHOU, J. & ZHANG, B. 2017.
427 Inhibition of HDAC6 increases acetylation of peroxiredoxin1/2 and ameliorates 6-OHDA induced
428 dopaminergic injury. *Neurosci Lett,* 658**,** 114-120.
429 JOCHEMS, J., BOULDEN, J., LEE, B. G., BLENDY, J. A., JARPE, M., MAZITSCHEK, R., VAN DUZER, J. H., JONES, S.
430 & BERTON, O. 2014. Antidepressant-like properties of novel HDAC6-selective inhibitors with
431 improved brain bioavailability. *Neuropsychopharmacology,* 39**,** 389-400.
432 KAPITEIN, L. C. & HOOGENRAAD, C. C. 2015. Building the Neuronal Microtubule Cytoskeleton. *Neuron,* 87**,**
433 492-506.
434 KOFLER, J., BELTRAN-QUINTERO, M. L., RUGARI, A., ZUCCOLI, G., KLOTZ, S. & ESCOLAR, M. L. 2022. Improved
435 Brain Pathology and Progressive Peripheral Neuropathy in a 15 Year Old Survivor of Infantile Krabbe
436 Disease Treated With Umbilical Cord Transplantation. *Front Mol Neurosci,* 15**,** 888231.
437 KRABBE, K. 1916. A new familial, infantile form of diffuse brain-sclerosis. *Brain,* 39**,** 74–114.
438 KREHER, C., FAVRET, J., WEINSTOCK, N. I., MAULIK, M., HONG, X., GELB, M. H., WRABETZ, L., FELTRI, M. L. &
439 SHIN, D. 2022. Neuron-specific ablation of the Krabbe disease gene galactosylceramidase in mice
440 results in neurodegeneration. *PLoS Biol,* 20**,** e3001661.
441 LEE, W. C., TSOI, Y. K., DICKEY, C. A., DELUCIA, M. W., DICKSON, D. W. & ECKMAN, C. B. 2006. Suppression of
442 galactosylceramidase (GALC) expression in the twitcher mouse model of globoid cell leukodystrophy
443 (GLD) is caused by nonsense-mediated mRNA decay (NMD). *Neurobiol Dis,* 23**,** 273-80.
444 LIN, D., DONSANTE, A., MACAULEY, S., LEVY, B., VOGLER, C. & SANDS, M. S. 2007. Central nervous system-
445 directed AAV2/5-mediated gene therapy synergizes with bone marrow transplantation in the murine
446 model of globoid-cell leukodystrophy. *Mol Ther,* 15**,** 44-52.
447 LOPRESTI, P. 2019. The Selective HDAC6 Inhibitor ACY-738 Impacts Memory and Disease Regulation in an
448 Animal Model of Multiple Sclerosis. *Front Neurol,* 10**,** 519.
449 MAJID, T., GRIFFIN, D., CRISS, Z., 2ND, JARPE, M. & PAUTLER, R. G. 2015. Pharmocologic treatment with
450 histone deacetylase 6 inhibitor (ACY-738) recovers Alzheimer's disease phenotype in amyloid
451 precursor protein/presenilin 1 (APP/PS1) mice. *Alzheimers Dement (N Y),* 1**,** 170-181.

452 MIYATAKE, T. & SUZUKI, K. 1972. Globoid cell leukodystrophy: additional deficiency of psychosine
453 galactosidase. *Biochem Biophys Res Commun,* 48**,** 539-43.
454 NOGUEIRA-RODRIGUES, J., BRITES, P. & SOUSA, M. M. 2016. Axonal pathology in Krabbe's disease: The
455 cytoskeleton as an emerging therapeutic target. *J Neurosci Res,* 94**,** 1037-41.
456 QIN, E. Y., HAWKINS-SALSBURY, J. A., JIANG, X., REDDY, A. S., FARBER, N. B., ORY, D. S. & SANDS, M. S. 2012.
457 Bone marrow transplantation increases efficacy of central nervous system-directed enzyme
458 replacement therapy in the murine model of globoid cell leukodystrophy. *Mol Genet Metab,* 107**,**
459 186-96.
460 RAFI, M. A., RAO, H. Z., LUZI, P. & WENGER, D. A. 2015. Long-term Improvements in Lifespan and Pathology
461 in CNS and PNS After BMT Plus One Intravenous Injection of AAVrh10-GALC in Twitcher Mice. *Mol*
462 *Ther,* 23**,** 1681-1690.
463 RIVIECCIO, M. A., BROCHIER, C., WILLIS, D. E., WALKER, B. A., D'ANNIBALE, M. A., MCLAUGHLIN, K., SIDDIQ,
464 A., KOZIKOWSKI, A. P., JAFFREY, S. R., TWISS, J. L., RATAN, R. R. & LANGLEY, B. 2009. HDAC6 is a
465 target for protection and regeneration following injury in the nervous system. *Proc Natl Acad Sci U S*
466 *A,* 106**,** 19599-604.
467 ROSSAERT, E., POLLARI, E., JASPERS, T., VAN HELLEPUTTE, L., JARPE, M., VAN DAMME, P., DE BOCK, K.,
468 MOISSE, M. & VAN DEN BOSCH, L. 2019. Restoration of histone acetylation ameliorates disease and
469 metabolic abnormalities in a FUS mouse model. *Acta Neuropathol Commun,* 7**,** 107.
470 SAKAI, N., INUI, K., TATSUMI, N., FUKUSHIMA, H., NISHIGAKI, T., TANIIKE, M., NISHIMOTO, J., TSUKAMOTO,
471 H., YANAGIHARA, I., OZONO, K. & OKADA, S. 1996. Molecular cloning and expression of cDNA for
472 murine galactocerebrosidase and mutation analysis of the twitcher mouse, a model of Krabbe's
473 disease. *J Neurochem,* 66**,** 1118-24.
474 SIDDIQI, Z. A., SANDERS, D. B. & MASSEY, J. M. 2006. Peripheral neuropathy in Krabbe disease: effect of
475 hematopoietic stem cell transplantation. *Neurology,* 67**,** 268-72.
476 SMITH, B., GALBIATI, F., CANTUTI-CASTELVETRI, L., GIVOGRI, M. I., LOPEZ-ROSAS, A. & BONGARZONE, E. R.
477 2011. Peripheral neuropathy in the Twitcher mouse involves the activation of axonal caspase 3. *ASN*
478 *Neuro,* 3**,** art:e00066.
479 SOURANDER, P. & OLSSON, Y. 1968. Peripheral neuropathy in globoid cel leucodystrophy (morbus Krabbe).
480 *Acta Neuropathol,* 11**,** 69-81.
481 SU, Q., LI, T., HE, P. F., LU, X. C., YU, Q., GAO, Q. C., WANG, Z. J., WU, M. N., YANG, D. & QI, J. S. 2021.
482 Trichostatin A ameliorates Alzheimer's disease-related pathology and cognitive deficits by increasing
483 albumin expression and Abeta clearance in APP/PS1 mice. *Alzheimers Res Ther,* 13**,** 7.
484 SUZUKI, K. & SUZUKI, K. 1995. The twitcher mouse: a model for Krabbe disease and for experimental
485 therapies. *Brain Pathol,* 5**,** 249-58.
486 TANAKA, K., NAGARA, H., KOBAYASHI, T. & GOTO, I. 1988. The twitcher mouse: accumulation of
487 galactosylsphingosine and pathology of the sciatic nerve. *Brain Res,* 454**,** 340-6.
488 TEIXEIRA, C. A., MIRANDA, C. O., SOUSA, V. F., SANTOS, T. E., MALHEIRO, A. R., SOLOMON, M., MAEGAWA, G.
489 H., BRITES, P. & SOUSA, M. M. 2014. Early axonal loss accompanied by impaired endocytosis,
490 abnormal axonal transport, and decreased microtubule stability occur in the model of Krabbe's
491 disease. *Neurobiol Dis,* 66**,** 92-103.
492 WENGER, D. A., RAFI, M. A. & LUZI, P. 1997. Molecular genetics of Krabbe disease (globoid cell
493 leukodystrophy): diagnostic and clinical implications. *Hum Mutat,* 10**,** 268-79.
494 WHITE, A. B., GIVOGRI, M. I., LOPEZ-ROSAS, A., CAO, H., VAN BREEMEN, R., THINAKARAN, G. &
495 BONGARZONE, E. R. 2009. Psychosine accumulates in membrane microdomains in the brain of
496 krabbe patients, disrupting the raft architecture. *J Neurosci,* 29**,** 6068-77.
497 WRIGHT, M. D., POE, M. D., DERENZO, A., HALDAL, S. & ESCOLAR, M. L. 2017. Developmental outcomes of
498 cord blood transplantation for Krabbe disease: A 15-year study. *Neurology,* 89**,** 1365-1372.
499 ZAKA, M. & WENGER, D. A. 2004. Psychosine-induced apoptosis in a mouse oligodendrocyte progenitor cell
500 line is mediated by caspase activation. *Neurosci Lett,* 358**,** 205-9.

This is a provisional file, not the final typeset article

ZILBERMAN, Y., BALLESTREM, C., CARRAMUSA, L., MAZITSCHEK, R., KHOCHBIN, S. & BERSHADSKY, A. 2009. Regulation of microtubule dynamics by inhibition of the tubulin deacetylase HDAC6. *J Cell Sci,* 122, 3531-41.

9 FIGURE LEGENDS

Figure 1. Western blot analysis of tissues from WT and Twitcher mice treated with ACY-738 from P0 until P9 or until and humane endpoints.
(A) Timeline of the experimental set-up of daily ACY-738 delivery from P0 to P9. (B-D) Western blot analysis of acetylated tubulin and α-tubulin in (B) brains, (C) optic nerves and (D) sciatic nerves of P9 WT and Twitcher mice untreated or treated with ACY-738 (upper panels) and respective quantifications (lower panels). Data represent mean ± SEM (*p<0.05, **p<0.01, ****p<0.0001, two-tailed unpaired t-test) of n=8-9 control Twitcher and n=8-10 ACY-738-treated Twitcher. (E) Timeline of the experimental set-up of daily ACY-738 delivery from P0 until humane endpoints. (F-H) Western blot analysis of acetylated tubulin and α-tubulin of (F) brains, (G) optic nerves and (H) sciatic nerves of WT and Twitcher mice untreated and treated with ACY-738 until humane endpoints were reached (upper panels) and respective quantifications (lower panels). Note that in the case of the brain (F), given the differences in treated and untreated animals, quantification in separate gels was done for untreated WT and Twitcher mice. Data represent mean ± SEM (*p<0.05, **p<0.01, two-tailed unpaired t-test) of n=3-4 control WT mice, n=4 ACY-738-treated WT mice, n=2-4 control Twitcher and n=4 ACY-738-treated Twitcher.

Figure 2. *In vitro* study on the effect of ACY-738 on microtubule dynamics and axonal transport.
(A) Quantification of microtubule growth speed of WT and Twitcher DRG neurons untreated and treated with ACY-738. Data represent mean ± SEM (****p<0.0001, one-way ANOVA followed by Tukey's multiple comparison test, 22-49 growth cones per condition). (B) Kymographs depicting the movement of EB3-GFP in WT and Twitcher DRG neurons untreated and treated with ACY-738. (C) Velocity of mitochondria transport of WT and Twitcher DRG neurons isolated from animals either untreated or treated with ACY-738 from P0 until humane endpoints (Twitcher) or similar age ranges (WT). (D) Kymographs depicting the movement of mitochondria in WT and Twitcher DRG neurons untreated and treated with ACY-738. Data represent mean ± SEM (*p<0.05, **p<0.001, two-tailed unpaired t-test) of n=4 control WT mice, n=4 ACY-738-treated WT mice, n=4 control Twitcher and n=3 ACY-738-treated Twitcher.

Figure 3. Functional analysis of Twitcher mice after ACY-738 treatment.
(A) Analysis of the natural behavior of Twitcher mice during ACY-738 treatment. Data represent mean ± SEM (*p<0.05, ***p<0.001, two-way ANOVA) of n=14 control Twitcher and n=10 ACY-738-treated Twitcher. (B) Analysis of the provoked behavior of Twitcher mice during ACY-738 treatment. Data represent mean ± SEM (*p<0.05, ***p<0.001, two-way ANOVA) of n=14 control Twitcher and n=10 ACY-738-treated Twitcher. (C) Analysis of the activity level of Twitcher mice during ACY-738 treatment. Data represent mean ± SEM (*p<0.05, ***p<0.001, two-way ANOVA) of n=14 control Twitcher and n=10 ACY-738-treated Twitcher. Results are only shown starting at P15 as no significant differences were found between treated and untreated animals before that timepoint.

Figure 4. Morphometric analysis of the optic and sciatic nerves of P9 WT and Twitcher mice treated with ACY-738.

(A) Representative microphotographs of optic nerve of P9 WT and Twitcher mice untreated or treated with ACY-738. (B) Density of myelinated axons (MF) in the optic nerve related to (A). Data represent mean ± SEM (*p<0.05, **p<0.01, two-tailed unpaired t-test) of n=7 control WT mice, n=4 ACY-738-treated WT mice, n=8 control Twitcher and n=8 ACY-738-treated Twitcher. (C) Quantification of myelin by determination of g-ratio in optic nerves of related to (A). Data represent mean ± SEM (*p<0.05, two-tailed unpaired t-test) of n=5 control WT mice, n=3 ACY-738-treated WT mice, n=5 control Twitcher and n=6 ACY-738-treated Twitcher. (D) Density of unmyelinated axons (UF) in the optic nerve related to (A). Data represent mean ± SEM (*p<0.05, two-tailed unpaired t-test) of n=6 control WT mice, n=5 ACY-738-treated WT mice, n=4 control Twitcher and n=6 ACY-738-treated Twitcher. (E) Representative microphotographs of sciatic nerve of P9 WT and Twitcher mice untreated or treated with ACY-738. (F) Density of myelinated axons (MF) in the sciatic nerve related to (E). Data represent mean ± SEM (*p<0.05, ***p<0.001, two-tailed unpaired t-test) of n=9 control WT mice, n=7 ACY-738-treated WT mice, n=8 control Twitcher and n=8 ACY-738-treated Twitcher. (G) Density of unmyelinated axons (UF) in the sciatic nerve related to (E). Data represent mean ± SEM (***p<0.001, two-tailed unpaired t-test) of n=6 control WT mice, n=5 ACY-738-treated WT mice, n=5 control Twitcher and n=4 ACY-738-treated Twitcher. Data represent mean ± SEM of n=4 control Twitcher and n=4 ACY-738-treated Twitcher. Scale bar: 1µm

Figure 5. Morphometric analysis of the optic nerve and sciatic nerve of Twitcher mice treated with ACY-738 from P0 until humane endpoints.
(A) Representative microphotographs of the optic nerve from WT and Twitcher mice untreated or treated with ACY-738 from P0 until humane endpoints (Twitcher) or of similar age ranges (WT). (B) Density of myelinated axons (MF) in the optic nerve related to (A). Data represent mean ± SEM (**p<0.01, two-tailed unpaired t-test) of n=6 control WT mice, n=7 control Twitcher and n=8 ACY-738-treated Twitcher. (C) Quantification of myelin by determination of g-ratio in optic nerves of untreated and treated WT and Twitcher mice. Data represent mean ± SEM (*p<0.05, two-tailed unpaired t-test) of n=5 control WT mice, n=5 control Twitcher and n=6 ACY-738-treated Twitcher. (D) Density of unmyelinated axons (UF) in the optic nerve related to (A). Data represent mean ± SEM (*p<0.05, **p<0.01, two-tailed unpaired t-test) of n=7 control WT mice, n=6 control Twitcher and n=7 ACY-738-treated Twitcher. (E) Representative microphotographs of sciatic nerve of WT and Twitcher mice untreated or treated with ACY-738 from P0 until humane endpoints (Twitcher) or similar age ranges (WT). (F) Density of myelinated axons (MF) in the sciatic nerve related to (E). Data represent mean ± SEM of n=7 control Twitcher and n=7 ACY-738-treated Twitcher. (G) Density of unmyelinated axons (UF) in the sciatic nerve related to (E). Data represent mean ± SEM of n=7 control Twitcher and n=7 ACY-738-treated Twitcher. Scale bar: 1µm

DATA AVAILABILITY STATEMENT

The original contributions presented in the study are included in the article/supplementary material. Further inquiries can be directed to the corresponding author.

ETHICS STATEMENT

This is a provisional file, not the final typeset article

588 All animals were handled and euthanized according to the European Union Directive 2010/63/EU and
589 the national Decreto-lei nº113-2013. The protocols here described have been approved by the i3S
590 Ethical Committee and by the Portuguese Veterinarian Board.

591

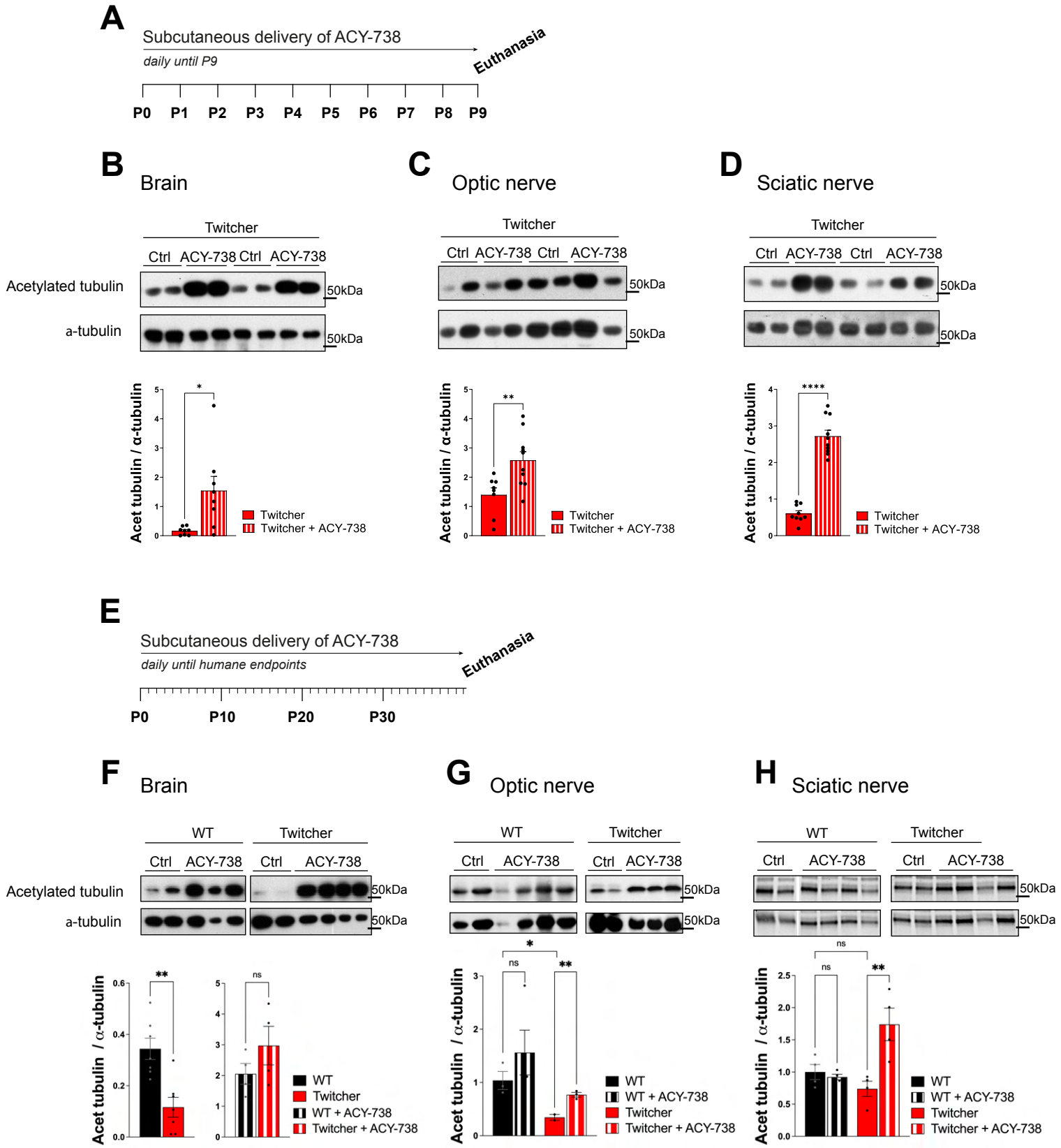
A
Subcutaneous delivery of ACY-738
daily until P9
Euthanasia
P0 P1 P2 P3 P4 P5 P6 P7 P8 P9
B
Brain
Twitcher
Ctrl ACY-738 Ctrl ACY-738
Acetylated tubulin
a-tubulin
50kDa
Acet tubulin / α-tubulin
Twitcher
Twitcher + ACY-738
C
Optic nerve
D
Sciatic nerve
E
Subcutaneous delivery of ACY-738
daily until humane endpoints
Euthanasia
P0 P10 P20 P30
F
Brain
WT
Twitcher
Ctrl ACY-738 Ctrl ACY-738
WT + ACY-738
G
Optic nerve
H
Sciatic nerve
ns

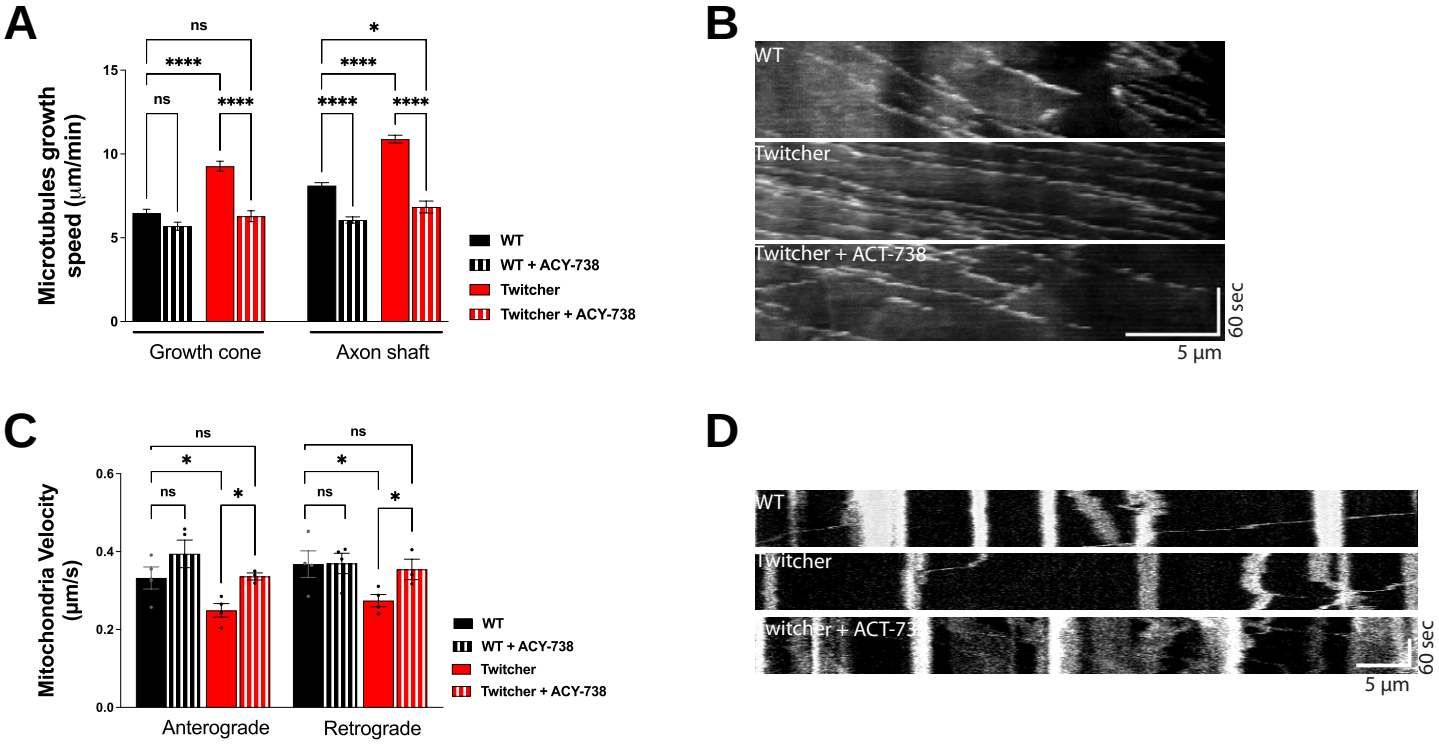
A
Microtubules growth speed (µm/min)
15
10
5
0
ns
****
ns
****
*
****
****
****
Growth cone
Axon shaft
WT
WT + ACY-738
Twitcher
Twitcher + ACY-738
B
WT
Twitcher
Twitcher + ACT-738
60 sec
5 µm
C
Mitochondria Velocity (µm/s)
0.6
0.4
0.2
0.0
ns
*
ns
*
ns
*
ns
*
Anterograde
Retrograde
WT
WT + ACY-738
Twitcher
Twitcher + ACY-738
D
WT
Twitcher
Twitcher + ACT-73
60 sec
5 µm

A

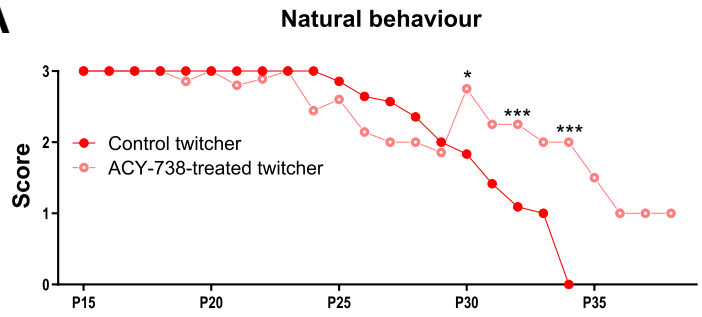

3	Normal
2	Minor changes
1	Less mobile but alert
0	Less mobile but not alert

B

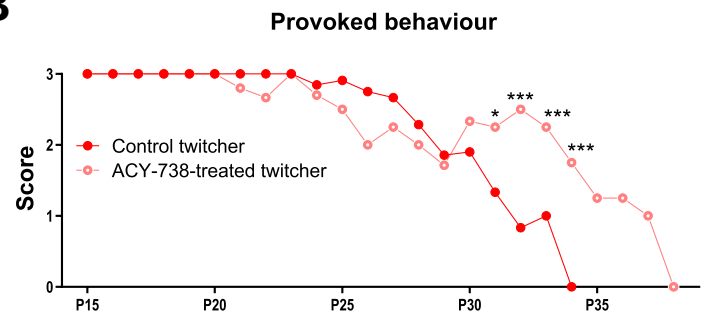

3	Normal
2	Minor changes
1	Moderate changes
0	Weakness and pre-comatose state

C

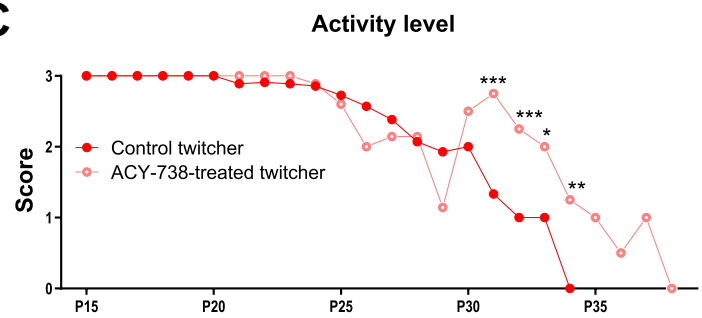

3	Normal
2	Mild decrease
1	Moderate decrease
0	Severely decreased

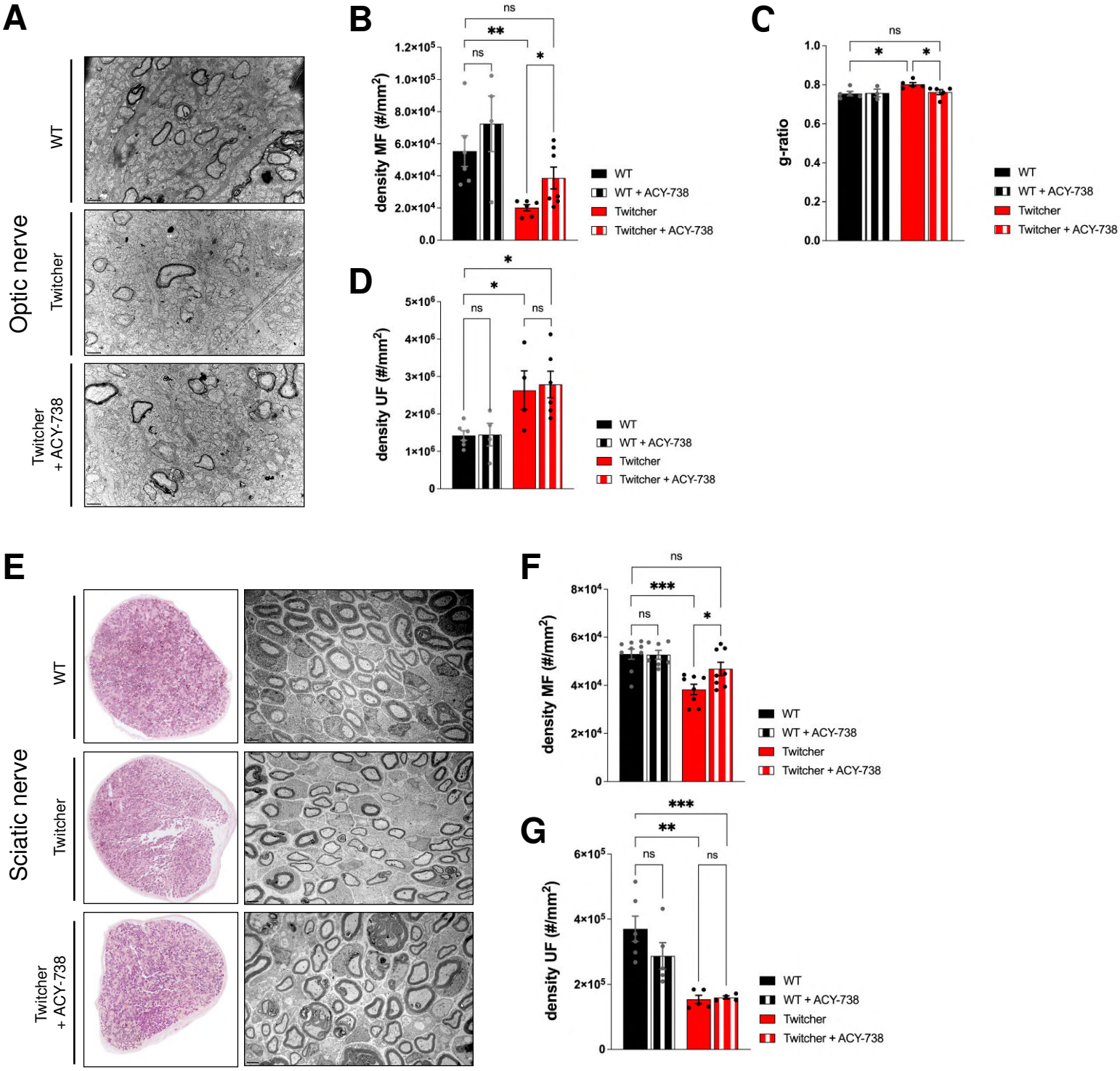
A
Optic nerve
WT
Twitcher
Twitcher + ACY-738
B
density MF (#/mm²)
1.2×10⁵
1.0×10⁵
8.0×10⁴
6.0×10⁴
4.0×10⁴
2.0×10⁴
0.0
ns
**
ns
*
WT
WT + ACY-738
Twitcher
Twitcher + ACY-738
C
g-ratio
1.0
0.8
0.6
0.4
0.2
0.0
ns
*
*
WT
WT + ACY-738
Twitcher
Twitcher + ACY-738
D
density UF (#/mm²)
5×10⁶
4×10⁶
3×10⁶
2×10⁶
1×10⁶
0
*
*
ns
ns
WT
WT + ACY-738
Twitcher
Twitcher + ACY-738
E
Sciatic nerve
WT
Twitcher
Twitcher + ACY-738
F
density MF (#/mm²)
8×10⁴
6×10⁴
4×10⁴
2×10⁴
0
ns
***
ns
*
WT
WT + ACY-738
Twitcher
Twitcher + ACY-738
G
density UF (#/mm²)
6×10⁵
4×10⁵
2×10⁵
0
***
**
ns
ns
WT
WT + ACY-738
Twitcher
Twitcher + ACY-738

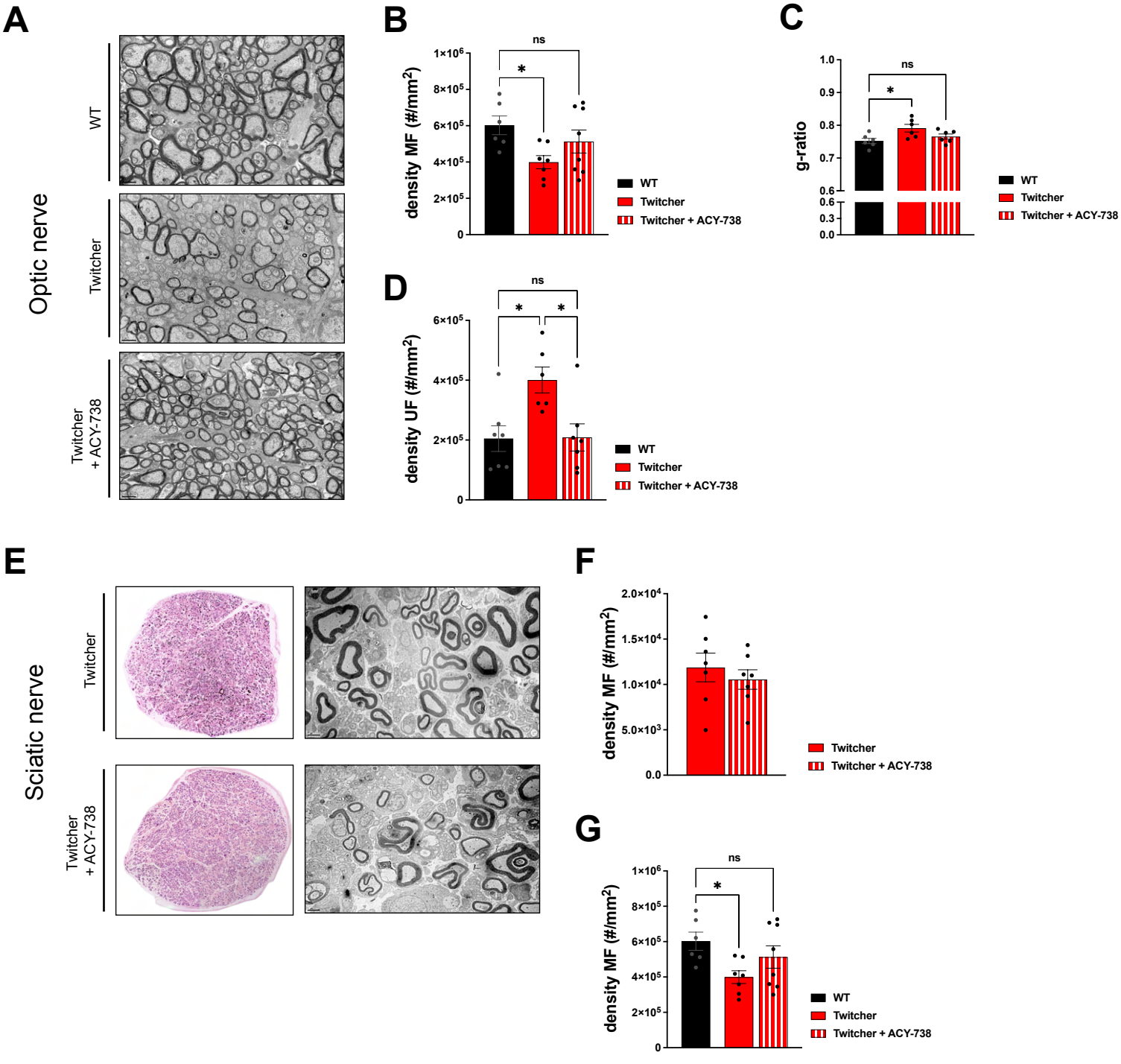
A
Optic nerve
WT
Twitcher
Twitcher + ACY-738
B
density MF (#/mm²)
1×10⁶
8×10⁵
6×10⁵
4×10⁵
2×10⁵
0
ns
*
WT
Twitcher
Twitcher + ACY-738
C
g-ratio
1.0
0.9
0.8
0.7
0.6
0.6
0.3
0.0
ns
*
WT
Twitcher
Twitcher + ACY-738
D
density UF (#/mm²)
6×10⁵
4×10⁵
2×10⁵
0
ns
*
*
WT
Twitcher
Twitcher + ACY-738
E
Sciatic nerve
Twitcher
Twitcher + ACY-738
F
density MF (#/mm²)
2.0×10⁴
1.5×10⁴
1.0×10⁴
5.0×10³
0.0
Twitcher
Twitcher + ACY-738
G
density MF (#/mm²)
1×10⁶
8×10⁵
6×10⁵
4×10⁵
2×10⁵
0
ns
*
WT
Twitcher
Twitcher + ACY-738